SPARSITY-DRIVEN IMAGE FORMATION AND SPACE-VARIANT FOCUSING FOR SAR

N. Özben Önhon and Müjdat Çetin

Faculty of Engineering and Natural Sciences, Sabancı University, Orhanlı, Tuzla, 34956 Istanbul, Turkey

ABSTRACT

In synthetic aperture radar (SAR) imaging, the presence of moving targets in the scene causes phase errors in the SAR data and subsequently defocusing in the formed image. The defocusing caused by the moving targets exhibits space-variant characteristics, i.e., the defocusing arises only in the parts of the image containing the moving targets, whereas the stationary background is not defocused. Considering that the reflectivity field to be imaged usually admits sparse representation, we propose a sparsity-driven method for joint SAR imaging and removing the defocus caused by moving targets. The method is performed in a nonquadratic regularization based framework by solving an optimization problem, in which prior information about both the scene and phase errors are incorporated as constraints.

Index Terms— Motion errors, phase errors, space-variant focusing, regularization, synthetic aperture radar, sparsity

1. INTRODUCTION

In synthetic aperture radar (SAR) imaging, uncertainties on the position of the sensing platform or on the motion of the targets in the underlying scene cause artifacts in the reconstructed image. Due to the inexact knowledge about the position of the SAR sensor, the time required for the transmitted signal to propagate to the scene center and back cannot be determined accuretely, which cause phase errors in the SAR data [1]. This type of phase errors cause space-invariant defocusing, i.e., the amount of the defocusing in the reconstructed image is same for all points of the scene. Moving targets in the scene cause defocusing in the reconstructed image as well. However, this defocusing needs to be corrected with a space-variant refocus algorithm, since the defocusing appears only around the positions of the moving targets whereas the stationary background is not defocused [2]. Therefore, autofocus techniques developed for space-invariant focusing cannot handle the defocusing arising in the imaging of a scene including multiple moving targets with different velocities. The cross-range component of the target velocity causes the image of the target to be defocused in the cross-range direction, whereas the range component causes shifting in the cross-range direction and defocusing in both cross-range and range directions [3]. The image of a target that experiences significant vibration is defocused in the cross-range direction as well [4]. The common approach to space-variant focusing is to partition the image into smaller subimages such that the error on each subimage is approximately space-invariant [3, 5]. After each of the small subimages is focused independently using one of the conventional space-invariant autofocus techniques, these subimages are combined together to obtain the focused image. These kinds of approaches are based on post-processing of the conventionally reconstructed image. However, we know that conventional imaging does not perform well in sparse aperture scenarios or when the data are incomplete. On the other hand, regularization-based image reconstruction has succesfully been applied to SAR imaging and it is shown that it has many advantages over conventional imaging [6]. These techniques can alleviate the problems in the case of incomplete data or sparse aperture. Moreover, they produce images with increased resolution, reduced sidelobes, and reduced speckle by incorporation of prior information about the features of interest and imposing various constraints (e.g., sparsity, smoothness) about the scene. Motivated by these observations and considering that in SAR imaging, the underlying field usually exhibits a sparse structure, we previosly proposed a sparsity-driven technique for joint SAR imaging and space-invariant focusing by using a nonquadratic regularization based framework [7, 8]. Here, extending this framework we propose a method for joint sparsity-driven imaging and *space-variant* focusing for correction of phase errors caused by target motion. This not only involves a nontrivial extension of the phase error estimation piece of our previous framework, but it also provides opportunities for incorporation of information about the expected spatial structure of the motion errors as well. In particular, in the new approach presented here, we not only exploit the sparsity of the reflectivity field, but we also impose a constraint on the spatial sparsity of the phase errors based on the assumption that motion in the scene will be limited to a small number of spatial locations. The method is based on minimization of a cost function of both the field and phase errors. The algorithm is iterative and each iteration involves two steps, first of which is for image formation and

This work was partially supported by the Scientific and Technological Research Council of Turkey under Grant 105E090, and by a Turkish Academy of Sciences Distinguished Young Scientist Award.

second is for phase error estimation. Successful results have been obtained in experiments involving synthetic scenes with simulated multiple targets.

2. SAR IMAGING MODEL

SAR is generally used for imaging of the ground from a plane or satellite. On its flight path, a SAR sensor transmits pulses to the ground and then receives the reflected signals. In most SAR applications, the transmitted signal is a chirp signal, which has the following form:

$$s(t) = Re\left\{\exp[j(\omega_0 t + \alpha t^2)]\right\} \tag{1}$$

Here, ω_0 is the center frequency and 2α is the so-called chirp-rate. The received signal $q_m(t)$ at a certain aperture position θ involves the convolution of the transmitted chirp signal with the projection $p_m(u)$ of the field at that observation angle.

$$q_m(t) = Re\left\{\int p_m(u)\exp[j[\omega_0(t-\tau_0-\tau(u)) + \alpha(t-\tau_0-\tau(u))^2]]du\right\} \tag{2}$$

Here, τ_0 represents the time required for the transmitted signal to propagate to the scene center and back. $\tau_0+\tau(u)$ is the delay for the returned signal from the scatterer at the range position d_0+u, where d_0 is the distance between the SAR sensor and the scene center. The data used for imaging are obtained after a pre-processing operation involving mixing and filtering steps. After this process, the relation between the field $F(x,y)$ and the pre-processed SAR data $r_m(t)$ becomes

$$r_m(t) = \iint\limits_{x^2+y^2\le L^2} F(x,y)\exp\{-jU(x\cos\theta + y\sin\theta)\}dxdy \tag{3}$$

where

$$U = \frac{2}{c}(\omega_0 + 2\alpha(t-\tau_0)) \tag{4}$$

and L is the radius of the illuminated area. All of the returned signals from all observation angles constitute a patch from the two dimensional spatial Fourier transform of the corresponding field. The corresponding discrete model including all returned signals is as follows.

$$\underbrace{\begin{bmatrix} r_1 \\ r_2 \\ \\ \\ r_M \end{bmatrix}}_{r} = \underbrace{\begin{bmatrix} C_1 \\ C_2 \\ \\ \\ C_M \end{bmatrix}}_{C} f \tag{5}$$

Here, r_m is the vector of observed samples, C_m is a discretized approximation to the continuous observation kernel at the $m-th$ cross-range position, f is a vector representing the unknown sampled reflectivity image and M is the total number of cross-range positions. The vector r is the SAR phase history data of all points in the scene. It is also possible to view r as the sum of the SAR data corresponding to each point in the scene.

$$r = \underbrace{C_{clmn-1}f(1)}_{rp_1} + \underbrace{C_{clmn-2}f(2)}_{rp_2} + .. + .. + \underbrace{C_{clmn-I}f(I)}_{rp_I} \tag{6}$$

Here, C_{clmn-i} is the $i-th$ column of the model matrix C and, $f(i)$ and rp_i represent the complex reflectivity at the $i-th$ point of the scene and the corresponding SAR data, respectively. I is the total number of points in the scene. Targets moving in cross-range direction or vibrating targets cause defocusing in the reconstructed image. The defocusing arises due to the phase errors in the SAR data of these targets. Let us assume the $i-th$ point in the scene as a point target moving in cross-range direction or vibrating without translation. The SAR data of this target can be expressed as:

$$\begin{bmatrix} rp_{i_{1_e}} \\ rp_{i_{2_e}} \\ . \\ . \\ . \\ rp_{i_{M_e}} \end{bmatrix} = \begin{bmatrix} e^{j\phi_i(1)}\ rp_{i_1} \\ e^{j\phi_i(2)}\ rp_{i_2} \\ . \\ . \\ . \\ e^{j\phi_i(M)}\ rp_{i_M} \end{bmatrix} \tag{7}$$

Here, ϕ_i represents the phase error in the cross-range direction caused by the motion of the target and, rp_i and rp_{i_e} are the phase history data for the stationary and moving point target, respectively. In a similar way, this relation can be expressed in terms of model matrix as follows:

$$\begin{bmatrix} C_{clmn-i_1}(\phi) \\ C_{clmn-i_2}(\phi) \\ . \\ . \\ . \\ C_{clmn-i_M}(\phi) \end{bmatrix} = \begin{bmatrix} e^{j\phi_i(1)}\ C_{clmn-i_1} \\ e^{j\phi_i(2)}\ C_{clmn-i_2} \\ . \\ . \\ . \\ e^{j\phi_i(M)}\ C_{clmn-i_M} \end{bmatrix} \tag{8}$$

Here, $C_{clmn-i}(\phi)$ is the i-th column of the model matrix $C(\phi)$ that takes the movement of the targets into account and $C_{clmn-i_m}(\phi)$ is the part of $C_{clmn-i}(\phi)$ for the $m-th$ cross-range position. In the presence of additional observation noise, the observation model for the overall system becomes

$$g = C(\phi)f + v \tag{9}$$

where, v is the observation noise. Here, the aim is to estimate f and ϕ from the noisy observation g.

3. PROPOSED METHOD

In the context of SAR imaging of man-made objects, the underlying scene, dominated by strong metallic scatterers, is usually sparse, i.e., there are few nonzero pixels. Based on that observation, we propose a sparsity-driven method

for joint estimation of the field and phase errors caused by the targets moving in the cross-range direction. The method is based on a nonquadratic regularization-based framework which allows the incorporation of the prior sparsity information about the field and about the phase error into the problem. The phase errors are incorporated to the problem using the vector β , which includes phase errors corresponding to all points in the scene, for all cross-range positions.

$$\beta = \begin{bmatrix} \beta_1 \\ \beta_2 \\ . \\ . \\ . \\ \beta_M \end{bmatrix} \tag{10}$$

Here, β_m is the vector of phase errors for the $m-th$ cross-range position and has the following form:

$$\beta_m = \left[e^{j\phi_1(m)}, e^{j\phi_2(m)}, ..., e^{j\phi_I(m)} \right]^T \tag{11}$$

The method is performed by minimizing the following cost function with respect to the field and phase errors.

$$\arg\min_{f,\beta} J(f,\beta) = \arg\min_{f,\beta} \|g - C(\phi)f\|_2^2 + \lambda_1 \|f\|_1 + \lambda_2 \|\beta - \mathbf{1}\|_1 \quad s.t. \quad |\beta(i)| = 1 \quad \forall i \tag{12}$$

Here, $\mathbf{1}$ is a $MI \times 1$ vector of ones. Since the number of moving points is much less than the total number of points in the scene, most of the ϕ values in the vector β are zero. Since the elements of β are in the form of $e^{j\phi}$'s, when ϕ is zero, β becomes one. Therefore, this sparsity on the phase errors is incorporated into the problem by using the regularization term $\|\beta - \mathbf{1}\|_1$. This problem is solved iteratively. In each iteration, in first step, the cost function $J(f,\beta)$ is minimized with respect to the field f.

$$\hat{f}^{(n+1)} = \arg\min_f J(f, \hat{\beta}^{(n)}) = \arg\min_f \left\| g - C^{(n)}(\phi) f \right\|_2^2 + \lambda_1 \|f\|_1 \tag{13}$$

This minimization problem is solved using the technique in [6]. Using the field estimate $\hat{f}$, in the second step, to estimate the phase errors imposed by the moving targets, the following cost function is minimized for each cross-range position:

$$\hat{\beta}_m^{(n+1)} = \arg\min_{\beta_m} J(\hat{f}^{(n+1)}, \beta_m) = \arg\min_{\beta_m} \left\| g_m - C_m T^{(n+1)} \beta_m \right\|_2^2 + \lambda_2 \|\beta_m - \mathbf{1}\|_1 \quad s.t. \quad |\beta_m(i)| = 1 \quad \forall i \tag{14}$$

Here, T is a diagonal matrix, with the entries $\hat{f}(i)$ on its main diagonal, as follows:

$$T^{(n+1)} = diag\left\{ \hat{f}^{(n+1)}(i) \right\} \tag{15}$$

In (14), $\mathbf{1}$ is a $I \times 1$ vector of ones. The constrained optimization problem in (14) is replaced with the following unconstrained problem that incorporates a penalty term on the magnitudes of $\beta_m(i)$'s.

$$\begin{aligned} \hat{\beta}_m^{(n+1)} &= \arg\min_{\beta_m} \left\| g_m - C_m T^{(n+1)} \beta_m \right\|_2^2 + \lambda_2 \|\beta_m - \mathbf{1}\|_1 + \lambda_3 \sum_{i=1}^{I} (|\beta_m(i)| - 1)^2 \\ &= \arg\min_{\beta_m} \left\| g_m - C_m T^{(n+1)} \beta_m \right\|_2^2 + \lambda_2 \|\beta_m - \mathbf{1}\|_1 + \lambda_3 \|\beta_m\|_2^2 - 2\lambda_3 \|\beta_m\|_1 \\ & \qquad m = 1, 2, ..., M \end{aligned} \tag{16}$$

This optimization problem is solved by using the same technique as in the field estimation step. Using the estimate $\hat{\beta}_m$, the following matrix is created,

$$B_m^{(n+1)} = diag\left\{ \hat{\beta}_m^{(n+1)}(i) \right\} \tag{17}$$

which is used to update the model matrix for the $m-th$ cross-range position.

$$C_m^{(n+1)}(\phi) = C_m B_m^{(n+1)} \tag{18}$$

After these phase estimation and model matrix update procedures have been completed for all cross-range positions, the algorithm passes to the next iteration, by incrementing n and rotating to (13).

4. EXPERIMENTAL RESULTS

We show experimental results on two different synthetic scenes. To demonstrate the effectiveness of and highlight the benefits specificly provided by the proposed method, for both experiments, the images reconstructed by conventional imaging (the polarformat algorithm [2]) and sparsity-driven imaging [6] are presented as well. In the first experiment, there are multiple moving targets in the scene. To simulate different motions and velocities of the targets, the phase history data of each target are corrupted by a different phase error function. The phase histories of the three point targets are corrupted by independent random phase error functions uniformly distributed in $[-\pi/2, \pi/2]$. The phase histories of the two bigger targets are corrupted by quadratic phase error functions of different peak values. In Figure 1, the results of the first experiment are displayed. In the second experiment, the scene is constructed so that it involves many stationary point targets and a strongly vibrating rigid-body target. To simulate it, the phase history data corresponding to each point of this target are corrupted by independent random phase error functions uniformly distributed in $[-\pi/2, \pi/2]$. The results of the second experiment are displayed in Figure 2. From the results for conventional imaging and sparsity-driven imaging without any phase error correction, the defocusing and artifacts in the reconstructed images caused by the

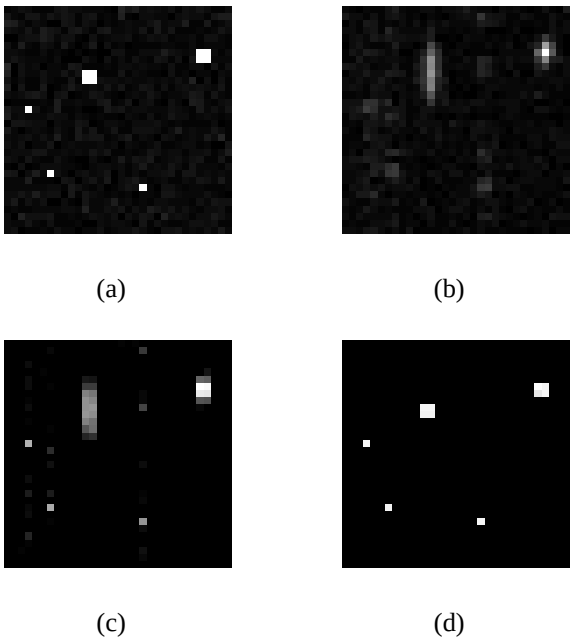

Fig. 1. a) Original scene. b) Image reconstructed by conventional imaging. c) Image reconstructed by sparsity-driven imaging. d) Image reconstructed by the proposed method.

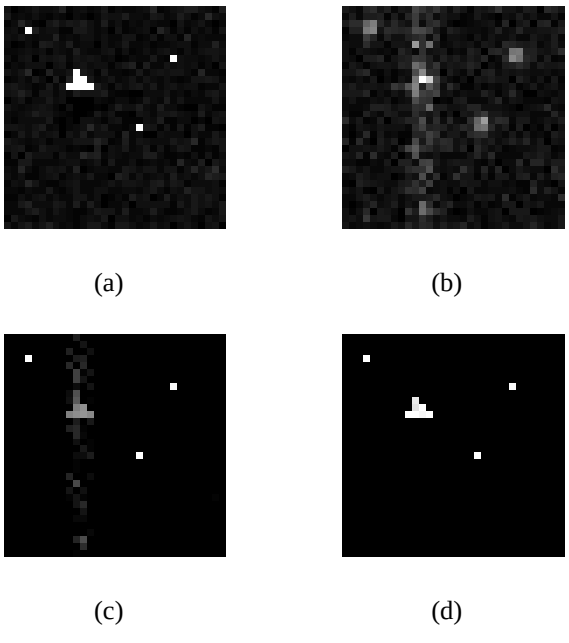

Fig. 2. a) Original scene. b) Image reconstructed by conventional imaging. c) Image reconstructed by sparsity-driven imaging. d) Image reconstructed by the proposed method.

moving targets are clearly seen. On the other hand, images reconstructed by the proposed method are well focused and show the advantages of sparsity-driven imaging such as high resolution, reduced speckle and sidelobes, as well as effective correction of the phase errors due to target motion.

5. CONCLUSION

We proposed a sparsity-driven method for joint imaging and correction of space-variant defocusing in SAR. The method effectively produces high resolution images and removes the cross-range dependent phase errors caused by moving targets. Moreover, the estimated phase errors can be used to estimate the velocity and characteristics of the motion. With slight extensions, the method is also applicable to range dependent phase errors imposed by moving targets. Our planned future work involves experiments on real SAR data.

6. REFERENCES

[1] C. V. Jakowatz, Jr., D. E. Wahl, P. H. Eichel, D. C. Ghiglia, and P. A. Thompson, *Spotlight-Mode Synthetic Aperture Radar: A Signal Processing Approach*, Springer, 1996.

[2] W. G. Carrara, R. M. Majewski, and R. S. Goodman, *Spotlight Synthetic Aperture Radar: Signal Processing Algorithms*, Artech House, 1995.

[3] C. V. Jakowatz, Jr., D. E. Wahl, and P. H. Eichel, "Refocus of constant velocity moving targets in synthetic aperture radar imagery," *Algorithms for Synthetic Aperture Radar Imagery V, SPIE*, 1998.

[4] A. R. Fasih, B. D. Rigling, and R. L. Moses, "Analysis of target rotation and translation in SAR imagery," *Algorithms for Synthetic Aperture Radar Imagery XVI, SPIE*, 2009.

[5] J. R. Fienup, "Detecting moving targets in SAR imagery by focusing," *IEEE Transactions on Aerospace and Electronic Systems*, vol. 37, no. 3, pp. 794–809, 2001.

[6] M. Çetin and W.C. Karl, "Feature-enhanced synthetic aperture radar image formation based on nonquadratic regularization," *IEEE Trans. Image Processing*, vol. 10, no. 4, pp. 623–631, 2001.

[7] N. Ö. Önhon and M. Çetin, "A nonquadratic regularization based technique for joint SAR imaging and model error correction," *Algorithms for Synthetic Aperture Radar Imagery XVI, Proc. SPIE*, vol. 7337, 2009.

[8] N. Ö. Önhon and M. Çetin, "Joint sparsity-driven inversion and model error correction for radar imaging," *IEEE Int. Conf. Acoustics, Speech, Signal Processing*, pp. 1206–1209, 2010.